Autocorrelation Analysis for the Unbiased Determination of Power-Law Exponents in Single-Quantum-Dot Blinking

Julien Houel,*,† Quang T. Doan,‡ Thomas Cajgfinger,‡ Gilles Ledoux,† David Amans,† Antoine Aubret,† Agnès Dominjon,‡ Sylvain Ferriol,‡ Rémi Barbier,‡ Michel Nasilowski,§ Emmanuel Lhuillier,§ Benoît Dubertret,§ Christophe Dujardin,† and Florian Kulzer*,†

†Institut Lumière-Matière, CNRS UMR5306, Université Lyon 1, Université de Lyon, 69622 Villeurbanne CEDEX, France, ‡Institut de Physique Nucléaire de Lyon, CNRS UMR5822, Université Lyon 1, Université de Lyon, 4 rue Enrico Fermi, 69622 Villeurbanne CEDEX, France, and §LPEM, ESPCI-ParisTech, PSL Research University, CNRS, Sorbonnes Université, UPMC Paris VI, 10 rue Vauquelin, 75005 Paris, France

ABSTRACT We present an unbiased and robust analysis method for power-law blinking statistics in the photoluminescence of single nanoemitters, allowing us to extract both the bright- and dark-state power-law exponents from the emitters' intensity autocorrelation functions. As opposed to the widely used threshold method, our technique therefore does not require discriminating the emission levels of bright and dark states in the experimental intensity timetraces. We rely on the simultaneous recording of 450 emission timetraces of single CdSe/CdS core/shell quantum dots at a frame rate of 250 Hz with single photon sensitivity. Under these conditions, our approach can determine ON and OFF power-law exponents with a precision of 3% from a comparison to numerical simulations, even for shot-noise-dominated emission signals with an average intensity below 1 photon per frame and per quantum dot. These capabilities pave the way for the unbiased, threshold-free determination of blinking power-law exponents at the microsecond time scale.

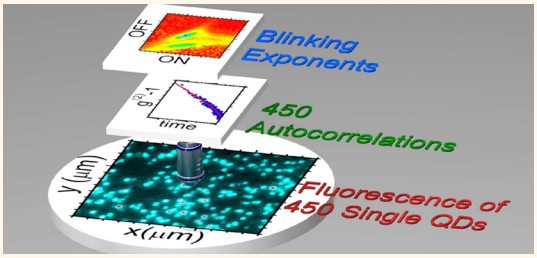

KEYWORDS: colloidal quantum dots · photoluminescence · power-law blinking · intensity autocorrelation · nonergodicity

Blinking, that is to say intermittent fluorescence,[1−4] is a ubiquitous feature of the emission of nanoparticles[5] and can have dramatic consequences for many potential applications. For colloidal quantum dots (QDs), blinking affects the performance of lasers,[6] light emitting diodes[7] and single photon sources.[8,9] Photoluminescence (PL) intermittence manifests itself as intensity fluctuations in the fluorescence timetrace of nanoemitters, where highly emitting states (ON states) are repeatedly interrupted by poorly emitting states (OFF states). The durations of these alternating ON and OFF periods are found to be distributed according to power laws for many kinds of quantum emitters,[5] including CdSe/CdS QDs. Given power-law blinking, the probability $P_{\mathrm{ON(OFF)}}(t)\,\mathrm{d}t$ of observing an ON (OFF) state duration between t and $t + \mathrm{d}t$ is governed by the probability density

$$P_{\mathrm{ON(OFF)}}(t) = (m_{\mathrm{ON(OFF)}} - 1)\cdot\theta^{m_{\mathrm{ON(OFF)}}-1}\cdot t^{-m_{\mathrm{ON(OFF)}}} \quad (1)$$

where $m_{\mathrm{ON(OFF)}}$ is the power-law exponent associated with the ON (OFF) state and θ is the cut-on time of the blinking process. For colloidal QDs, power law exponents $\lesssim 2$ have been found, which implies nonergodicity of the ON- and OFF-state dynamics.[10,11]

Theoretical efforts to explain power-law-like emission characteristics started with Randall and Wilkins, who showed that the existence of electron traps with exponentially distributed depths explains power-law decay of phosphorescence;[12] a similar scenario can explain power-law-distributed OFF-state dynamics of colloidal QDs. Power-law distributed ON times, however, are less straightforward to explain and more elaborate models had to be developed, based on spectral diffusion,[4,13] fluctuating barriers,[14,15] the existence of charged ON states,[16] spatial diffusion,[17] and variations of nonradiative rates.[18] While each of these models reproduces a large part of the available experimental evidence, there is still no unified approach that explains all observed

* Address correspondence to julien.houel@univ-lyon1.fr, florian.kulzer@univ-lyon1.fr.

Received for review November 20, 2014 and accepted December 30, 2014.

Published online December 30, 2014
10.1021/nn506598t

properties of QD fluorescence intermittency. Moreover, the existing models predict different power-law exponents. As a consequence, an accurate and reliable method to determine power-law exponents from experimental data appears to be crucial for a unified understanding of the underlying physical phenomena.

Several sophisticated methods exist for the analysis of single-nanoemitter blinking,[19] which usually proceed by first identifying the ON and OFF periods in single-particle fluorescence timetraces and then adjusting eq 1 to the probability densities of the observed ON and OFF times.[3,4,14,20] The standard procedure of least-squares fitting is known to have problems with long-tailed distributions.[21] Thus, more suitable methods to extract $m_{ON(OFF)}$ have been developed, based on maximum-likelihood criteria and other statistical tests.[21−24]

Nevertheless, all these approaches still crucially depend on a reliable distinction between ON and OFF in the emission intensity traces, which involves establishing an acceptable intensity threshold for a binned timetrace. The nanoemitter is thus considered to be in the ON-state if the intensity of a time bin surpasses this threshold and to be in the OFF-state otherwise, which is straightforward in both concept and implementation. However, it has been shown recently[25] that the extracted m_{ON} and m_{OFF} can differ by up to 30%, depending on the experimental resolution (bin time) and the chosen threshold value. Furthermore, this method obviously depends on the signal-to-noise ratio (SNR) and thus breaks down when the signals are dominated by shot noise, which blurs the distinction between ON and OFF levels and thus limits the temporal resolution that can be achieved.

The change-point detection approach of Watkins *et al.*[26] is an alternative to the threshold method, which works directly on photon arrival times without binning. However, a trade-off still exists between efficiency (detecting all state changes, avoiding false negatives) and purity (detecting only "real" state changes, avoiding false positives). This constraint reintroduces a user-biased choice for the acceptable level of false positives, with a concomitant trade-off for false negatives, in the maximum-likelihood analysis.

Two approaches, based on the analysis of the intensity power spectrum[27,28] or the intensity autocorrelation,[29,30] have been explored for extracting m_{ON} and m_{OFF} without trying to differentiate ON and OFF states explicitly in the timetrace. These methods successfully recover the power-law exponent if only one power-law process is at work, but become ambiguous as soon as two such distributions are involved, as is the case for QD blinking. In particular, Verberk *et al.*[30] present an analysis based on the fluorescence intensity autocorrelation function, which makes use of the full information contained in the delays between all pairs of detected photons. As such, a correlation-based analysis is less sensitive to noise, can be applied to the data at full temporal resolution, and does not require any ON/OFF intensity threshold to be defined. However, the autocorrelation function contains intermixed information on m_{ON} and m_{OFF}; so far no general analytical expression to extract m_{ON} and m_{OFF} from autocorrelation functions has been put forward.

In this article, we unravel this situation and present the first unbiased determination of m_{ON} and m_{OFF} power-law blinking exponents of CdSe/CdS QDs using the autocorrelation function, which does not require setting an intensity threshold for distinguishing ON and OFF states in the experimental emission timetrace, thus removing the potential bias[25] inherent in making such a choice. Our approach is robust with respect to experimental noise and temporal resolution, allowing the extraction of power-law exponents from fast (2 ms integration time), low-signal (<1 photon per frame for each QD on average) blinking data. Furthermore, our technique can easily be extended to photophysical schemes that involve more than two states and we therefore expect it to be applicable to many different types of blinking nanoemitters (*e.g.*, single molecules, nanowires, nanorods, *etc.*).

RESULTS AND DISCUSSION

The lack of a typical time scale in power-law blinking has dramatic consequences: To obtain complete information on the fluorescence dynamics of single nanoemitters, the total experimental time needs to be infinite. As a consequence, experimental autocorrelation functions, even of one and the same nanoemitter, recorded at different times can deviate from each other significantly. This is not necessarily due to any change in the blinking behavior (the underlying power-law exponents themselves), but rather an intrinsic signature of the nonergodicity (statistical aging) of luminescence that is governed by power-laws.[10,11] We therefore record a large number of single QD fluorescence timetraces simultaneously so that we can perform a statistical analysis of the corresponding autocorrelation functions; a subsequent comparison to numerical simulations identifies the best-fit power-law exponents with high specificity. To this end, we used a home-built wide-field microscope coupled to a fast electron-bombarded CMOS (ebCMOS) camera (see Methods and Figure 1a), allowing us to record the fluorescence of 450 single QDs simultaneously at a frame rate of 250 Hz with a total integration time of 660 s. It is worth mentioning that this frame rate is achieved on the full ebCMOS camera chip of 800 × 800 pixels. To our knowledge, this is the first report of such a large number of single QD timetraces recorded simultaneously at such a high frame rate and with the single photon sensitivity. (Section 16 of the Supporting

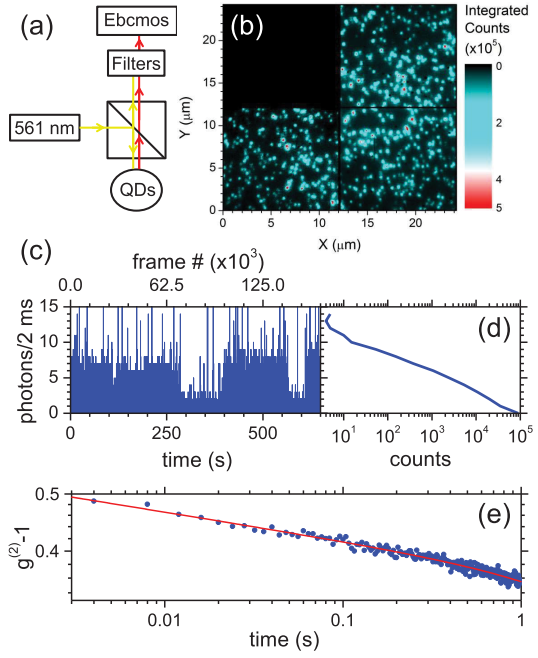

Figure 1. (a) Scheme of the experimental setup: Single QDs are excited at 561 nm with a continuous-wave laser, and their photoluminescence is collected through the excitation objective and directed onto an ebCMOS camera; scattered laser light is suppressed by long-pass filters. (b) Position-dependent integrated photon counts per pixel on a false-color scale; the total acquisition time was 660 s. (The black square in the top left is due to one of the 4 camera quadrants having been turned off during the measurement.) (c) An example of a single QD timetrace extracted from (b). (d) Distribution of the counts of the QD timetrace: no global threshold can be established to discriminate between the ON and OFF states at full temporal resolution (2 ms). (e) Autocorrelation function of the data in (c) (blue dots) and the corresponding fit of eq 3 (red line) with parameters $A = 0.37$, $B = 0.047$, and $C = 0.049$.

Information shows how our technique can be adapted to standard emCCD cameras.) To validate our method beyond standard conditions (slow acquisition and relatively high SNR), we deliberately kept the excitation power to a minimum, resulting in single-QD timetraces with average count rates of ~1 photon per frame. Such low-level signals can be recorded with the ebCMOS sensor thanks to its ultralow dark noise of less than 0.02 photons/QD/frame (see Supporting Information, Figure S9). Figure 1 b shows the integrated image of the emission of 450 individual QDs, to which a pattern recognition algorithm was applied to locate the positions of the QDs (see Supporting Information, Section 2). The signal of each QD was then extracted from the sequence of images as a 165 000-frame timetrace, an example of which is shown in Figure 1c. As can be seen in Figure 1d, the distribution of photon counts as commonly used in threshold-based methods[21−24] does not allow for the discrimination between ON and OFF states.

To analyze the single-QD timetraces, their fluorescence intensity autocorrelation functions $g^{(2)}(\tau)$ are calculated according to

$$g^{(2)}(\tau) = \frac{\langle I(t)I(t+\tau)\rangle}{\langle I(t)\rangle^2} \quad (2)$$

where $I(t)$ is the intensity (counts per timebin) at time t and $\langle\cdot\rangle$ represents time averages; Figure 1e shows an example of a single-QD autocorrelation function. Power-law blinking with exponents $m < 2$ leads to timetraces that are dominated by long events whose duration is of the same order of magnitude as the total measurement time.[31] As a consequence, the normalization factor $\langle I(t)\rangle^2$ in eq 2 does not tend toward a well-defined long-time limit. The experimental autocorrelation functions therefore show significant variation from one QD to the next, and even if one and the same QD is probed several times under identical experimental conditions. Nonetheless, the autocorrelation functions exhibit a well-defined general shape for almost all (more than 95%) of the 450 QDs we studied: a power-law decay modulated by an exponential cutoff, in accordance with earlier reports.[30] The red line in Figure 1e shows a fit of the autocorrelation $g^{(2)}(\tau) - 1$ with the following equation:

$$f(t) = At^{-C}\exp(-Bt) \quad (3)$$

where A represents the autocorrelation contrast, B is the cutoff time, and C is the power-law exponent of the autocorrelation function; C is equal to $2 - m$ if only one of the two states has lifetimes governed by a power law with exponent m.[30,31] Generally speaking, the decay of an autocorrelation function represents a loss of information about the state of the emitter: As time progresses, it becomes increasingly likely that transitions occur, and at long times one can only make general statistical predictions that are independent of the emitter's state at time $t = 0$. We can therefore surmise that the fit parameter C will be linked to the combined contributions of the m_{ON} and m_{OFF} distributions, given that both types of transitions are stochastic in nature and hence lead to information loss. The autocorrelation contrast A is influenced by the relative duration of the ON/OFF periods;[19] traces dominated by long OFF periods have higher correlation contrasts than those of an emitter that is mostly in the ON state. The exponential cutoff rate given by parameter B, a phenomenological addition to the fit function,[30] may be attributable, at least partially, to the finite measurement time.

On the basis of the above heuristic arguments, we conclude that the combination of parameters C and A may contain sufficient information to unravel the contributions of m_{ON} and m_{OFF}, even in the absence of a general analytical formula relating the fit parameters to the power-law exponents. (The cutoff parameter B can serve as a consistency check, see Supporting Information, Section 8.) Due to the nonergodicity of power-law

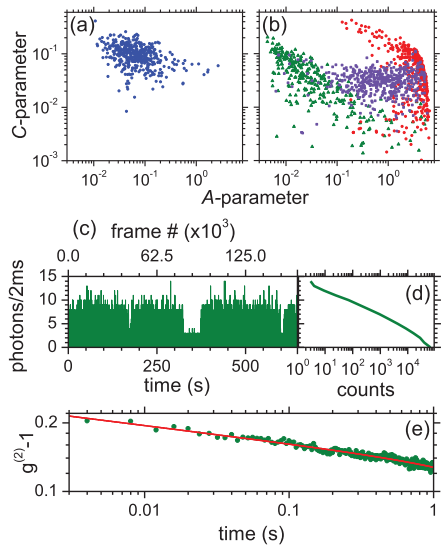

Figure 2. (a) 2D distribution of the (*A*,*C*) couples resulting from fitting eq 3 to the experimental autocorrelation functions. Our analysis relies on reproducing this 2D distribution with simulated power-law blinking timetraces that are subjected to the same autocorrelation analysis. (b) Three different (*A*,*C*) distributions obtained after fitting the autocorrelation functions of simulated traces for three different sets of (m_{ON},m_{OFF}) exponents. Green triangles correspond to (1.5,1.7), violet squares to (1.7,1.7) and red dots to (1.7,1.5). Every pair of exponents generates its characteristic 2D distribution in (*A*,*C*) space. (c) Example of a simulated timetrace with (m_{ON} = 1.80,m_{OFF} = 1.95) power-law exponents. (d) Distribution of the photon counts of the timetrace in (c). As for the experimental data, no global threshold can be established for discriminating ON and OFF states. (e) The corresponding autocorrelation (green dots), fitted (red line) by eq 3 with adjusted parameters *A* = 0.13, *B* = 0.056. and *C* = 0.079.

blinking, we expect to find a broad distribution of the two parameters in (*A*,*C*) space; Figure 2a shows that this is indeed the case for the 450 experimental autocorrelation functions. The hypothesis at the heart of our subsequent analysis is that this 2D distribution of the (*A*,*C*) parameters corresponds to one and only one (m_{ON},m_{OFF}) pair of blinking exponents. To validate this assumption, we have simulated 450 single QD timetraces with ON and OFF periods distributed according to power laws with exponents (m_{ON},m_{OFF}) (further details of the simulations and the fitting procedure are given in the Supporting Information, Sections 3 to 5). Figure 2c shows an example of a simulated timetrace for (m_{ON},m_{OFF}) = (1.8,1.95) and Figure 2e presents the corresponding autocorrelation. For every (m_{ON},m_{OFF}) couple, the 450 simulated autocorrelation functions are fitted with eq 3, yielding the 2D distribution of *A* and *C* in each case.

Three examples of such simulated distributions are plotted in Figure 2b for (m_{ON},m_{OFF}) = (1.5,1.7), (1.7,1.7) and (1.7,1.5). As expected, the distributions for each (m_{ON}, m_{OFF}) pair are spread over a large area in (*A*,*C*) space, meaning that correctly identifying the underlying power-law exponents requires studying a statistically significant number of single QDs (see Supporting Information, Section 12). Given a large-enough data set, we can test whether a single (m_{ON},m_{OFF}) couple can be identified as the "best fit" for describing the experimental data of Figure 2a. To this end, we use a 2D Kolmogorov–Smirnov (K–S) statistical test,[32,33] which compares the 2D (*A*,*C*) distributions of two different data sets, yielding a parameter *D* that quantifies the mismatch between the two distributions: $D \in [0,1]$, where $D = 0$ would correspond to prefect overlap. In total, we have tested 1444 different (m_{ON},m_{OFF}) combinations ranging from (1.05,1.05) to (2.9,2.9), covering more than the spread of values reported in the literature.[22,34,5,35,36,24] That is to say, we have simulated 450 single-QD timetraces for each (m_{ON},m_{OFF}) couple, determined the corresponding 2D distribution in (*A*,*C*) space and calculated the K–S parameter *D* with respect to the experimental data of Figure 2a. The 2D contour plot in Figure 3a shows the resulting values of *D* on a color scale as a function of m_{ON} and m_{OFF}; the high contrast of *D* spans variations of 1 order of magnitude, from $D \simeq 0.1$ to 1. There is an isolated, well-defined minimum of $D \lesssim 0.1$ at (1.8,1.95), indicating that a singular, narrowly delimited combination of exponents optimizes the overlap between the experimental data and simulations based on the power-law model of eq 1. A high-resolution contour plot of the parameter space around the minimum of *D* can be seen in Figure 3c. For this particular ensemble of CdSe/CdS QDs, we thus find best-fit blinking exponents of (m_{ON} = 1.805, m_{OFF} = 1.955) for the pixel with minimum *D*; the corresponding simulated (*A*,*C*) distribution is compared to the experimental data in Figure 3d.

After having shown that our approach can identify the optimal (m_{ON},m_{OFF}) couple with high specificity, we now discuss to what extent the autocorrelation analysis allows us to judge whether the underlying hypothesis itself—QD blinking is governed by power-law distributed probabilities, eq 1—is justified. To explore this issue, we took a simulated data set for (m_{ON} = 1.805,m_{OFF} = 1.955), *i.e.*, an ensemble of timetraces for which we know the null hypothesis to be true, and we subjected this set to the same analysis as the experimental data. We can thus identify the behavior of *D* that corresponds to genuine power-law blinking and quantify the degree of variation in *D* that is inherent in repeatedly probing the same power-law distributions with limited sample sizes and measurement times. As can be seen in Figure 3b, the resulting "ideal" contour plot agrees very well with the experimental one of Figure 3a, down to the shape of the faint offshoots observed for the main and secondary minima. However, the values of *D* are slightly lower in the minimum regions of Figure 3b, although this is barely noticeable given the color scale. We further investigated this point by subjecting both the real and the idealized (simulated) data to 215 different analysis

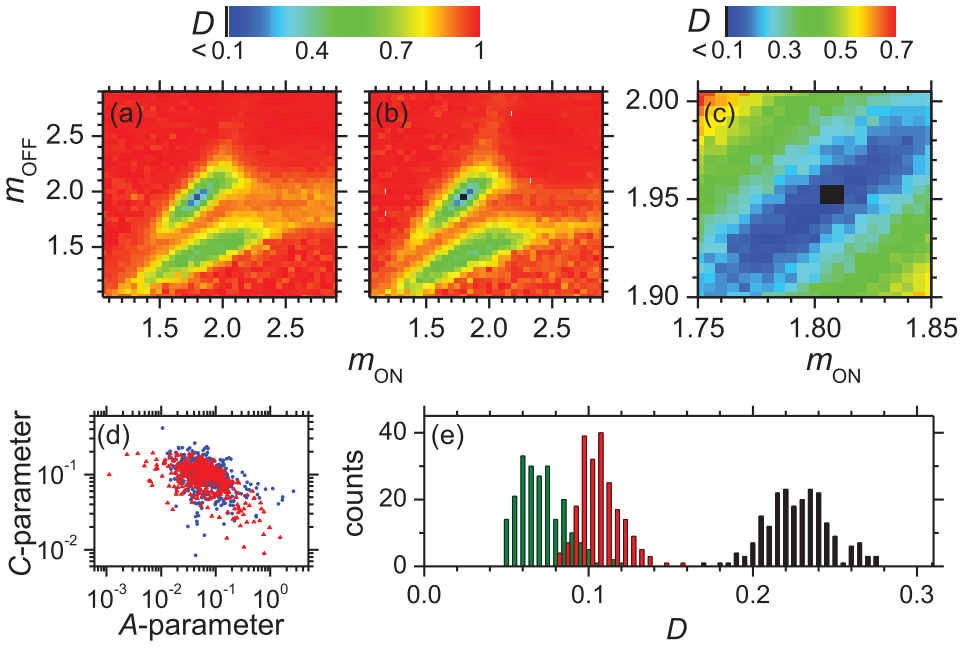

Figure 3. (a) Low-resolution comparison of simulations to experimental data with a 2D Kolmogorov–Smirnov (K–S) test. The K–S parameter *D* (color scale) is represented as a function of the m_{ON} and m_{OFF} exponents used in the simulations. There is a single (m_{ON}, m_{OFF}) couple, (1.80, 1.95), that minimizes the *D*-parameter, corresponding to the best agreement between experimental and simulated (*A*,*C*) distributions. (b) Same comparison as in (a), now with a simulated set for (m_{ON} = 1.80,m_{OFF} = 1.95) replacing the experimental data; all features of the original contour plot (a) are reproduced. (c) High-resolution exploration of the area of minimal *D* from (a), yielding more accurate optimum values of (m_{ON} = 1.805,m_{OFF} = 1.955) ± 3%. (d) 2D distributions of *A* and *C* for the data (blue dots, same as in Figure 2a) and the best-fit simulation (m_{ON} = 1.805,m_{OFF} = 1.955) (red triangles). (e) Reproducibility and distinctiveness of *D*: The red histogram shows the distribution found for *D* when comparing the experimental (*A*,*C*) distribution to 215 different analysis runs for the previously determined optimum couple (m_{ON} = 1.805,m_{OFF} = 1.955), while the black bars represent the analogous distribution for (m_{ON} = 1.85,m_{OFF} = 2.00), the second-lowest pixel in the contour plot in (a). The green histogram corresponds to a null-hypothesis calibration, for which one simulation run for (m_{ON} = 1.805,m_{OFF} = 1.955) is compared to 215 additional runs for the very same pair of parameters.

runs for the previously identified optimum parameters (m_{ON} = 1.805,m_{OFF} = 1.955). Each analysis run is based on a new seed of the random number generator and therefore produces its own simulated (*A*,*C*) distribution, to which both data sets (real and idealized) are then compared with the K–S test. The intersimulation comparisons thus yield the distribution of *D* values that can be expected for idealized power-law blinking, which, as is shown in Figure 3e (green histogram), has its mean value at D_{sim} = 0.074 with a standard deviation of σ_{sim} = 0.014. The experiment-simulation analysis runs, on the other hand, produce a roughly Gaussian-shaped histogram (red) with mean value D_{exp} = 0.107 and standard deviation σ_{exp} = 0.013. There is about 20% overlap between the experiment-simulation and the simulation-simulation distributions, with the *D* values for the experimental data being larger in general. This means that the data, on average, tends to agree slightly less well with simulations than can be expected from the variations between equivalent simulation-simulation analysis runs. Nevertheless, the large overlap means that there is no reason to reject the null hypothesis at the base of our analysis, which supposed that the blinking behavior of all the investigated QDs can be modeled by a power law with a single (m_{ON},m_{OFF}) combination. The remaining small offset between D_{exp} and D_{sim} might be due to an aspect of the particles' photophysics that is not incorporated in our model. For example, small inhomogeneities may be present in the investigated sample of 450 QDs as far as power-law exponents, the exciton emission rates and/or the ratios between bright and dark state emission efficiencies are concerned.

The black histogram in Figure 3e is the result of the experiment-simulation comparison for (m_{ON} = 1.85, m_{OFF} = 2.00), which corresponds to the pixel with the second-lowest *D* in the contour plot of Figure 3a. There is strictly no overlap with the *D* distribution for the optimum fit parameters (red histogram), illustrating once more the specificity of the autocorrelation analysis. In fact, as is detailed in the Supporting Information (Sections 8 and 10), we find that all 8 nearest-neighbor pixels in Figure 3a exhibit distributions whose maxima differ by at least 6σ from the mean value of *D* = 0.107 of the optimum-solution histogram (red); σ stands for the largest standard deviation of the compared histograms (worst case scenario). We therefore conclude that we are able to extract the power-law exponents with an absolute precision of ±0.05 (±3%) at 6σ specificity. The combination of m_{ON} = 1.805 with an almost 10% larger m_{OFF} = 1.955 indicates that these

QDs spend most of the time in the ON state under continuous illumination, a typical feature of such large-shell CdSe/CdS QDs.[35,37] It is particularly noteworthy that m_{OFF} approaches the critical threshold of 2, above which the average duration of the OFF periods becomes finite. The power-law exponent of the ON periods, on the other hand, is associated with an infinite average length; overall, this leads to a favorable interplay of ON *versus* OFF periods in the photoluminescence of this type of QD.

To complete the discussion of our technique, we now address its robustness with respect to two critical factors. First, we consider the influence of the ON/OFF intensity contrast. OFF states can still be moderately emissive ("dim" instead of completely dark), which makes it harder to distinguish them from the ON states. In fact, residual OFF state emission manifests itself in the contour plot of Figure 3a, which shows, besides the global minimum of $D = 0.1$, as a second domain (green) of relatively low D values around 0.4. This secondary minimum arises due to the relatively high quantum yield of the dark state for this type of QD, reaching 10% of the bright state emission. We show in the Supporting Information (Section 15) that this region shifts as a function of the dark state emissivity and tends to vanish if this emissivity drops below ~0.1% of the efficiency of the bright state. With regard to more emissive "dark" states, we verified (see Supporting Information, Section 14) that our technique maintains a precision of ±0.05 (under the experimental conditions discussed in this work) as long as dark state efficiencies stay below 50% of the bright states. As a consequence, the approach is also suitable for analyzing recently developed types of giant-shell[37−39] or alloyed QDs,[40] both of which have a high dark-state-emission efficiency.

The second important benchmark is the interplay between count rate, temporal resolution and residual uncertainty for the power-law exponents, which is linked to the sensitivity of the D parameter. As discussed above, we are able to extract the power-law exponents with an absolute precision of ±0.05 (±3%) at 6σ specificity. It is worth noting that this precision is achieved with shot-noise-dominated timetraces, well below saturation of the QD emission. Such minimally invasive conditions are preferable to approaches that require high count rates to discriminate between ON and OFF states, and hence high excitation intensities that may influence the blinking parameters,[41,42] for example due to multiphoton excitation of long-lived intermediate states, and can furthermore lead to photobleaching. As far as temporal resolution is concerned, our method can extract blinking power-law exponents for timetraces with only 0.1 photons/QD/frame on average, with a reasonable acquisition time T_{max} = 66 s with 3% precision (±0.05) at 6σ specificity (see Supporting Information, Section 13). This robustness against noise can be expected to allow blinking studies at up to 100 kHz (10 μs resolution), 1 order of magnitude faster than what has been demonstrated with change-point detection.[26] Verifying power-law behavior at the fastest possible time scale will be useful to elucidate the role of the cut-on time, θ in eq 1. Taking a pragmatic point of view, this cut-on time can be equated with the experimental temporal resolution; nevertheless, a more fundamental approach can be expected to improve our understanding of QD photophysics, for example, if a time scale can be identified at which the power-law behavior breaks down; in fact, some models predict the existence of such an onset time[12] or of a threshold time below which the power-law exponents change.[28]

CONCLUSIONS

We have presented a technique to determine unbiased power-law exponents of blinking CdSe/CdS core/shell QDs with a precision of 3% at 6σ specificity. To our knowledge, this constitutes the first approach for extracting the full set of blinking parameters from experimental autocorrelation functions, bypassing the need of introducing a possibly biased ON/OFF threshold. Our autocorrelation analysis is robust in the presence of noise and intrinsically free from timebin-dependent thresholding artifacts. As such, the method is capable of determining m_{ON} and m_{OFF} from timetraces dominated by shot noise, which are untreatable by other methods. We thus can extract the power-law exponents from ultralow signal data (~0.1 photon/frame/QD) with a precision of 3%, which offers the perspective of threshold-free blinking analysis at the microsecond time scale.

METHODS

CdSe/CdS Quantum Dot Synthesis. *Chemicals.* Methanol (VWR, 100%), ethanol (CarloErba, 99.5%), cadmium oxide (CdO) (Aldrich 99;99%), sulfur powder (Sigma-Aldrich, 99.998%), selenium powder (Sigma-Aldrich, 99.99%), cadmium nitrate tetrahydrate ($Cd(NO_3)_2(H_2O)_4$) (Sigma-Aldrich 99.999%), cadmium acetate dihydrate ($Cd(OAc)_2(H_2O)_2$) (Sigma-Aldrich, 98%), sodium hydroxide (Sigma-Aldrich, 97%), *n*-hexane (VWR, 98%), 1-octadecene (ODE, Sigma-Aldrich, 90%), oleylamine (Sigma-Aldrich, 70%), oleic acid (Sigma-Aldrich, 90%), myristic acid (Sigma-Aldrich) chemical were used as received, except for the oleylamine, which was centrifuged before use.

Preparation of Cadmium Myristate ($Cd(Myr)_2$). In a 1 L Erlenmeyer flask, 3.2 g (80 mmol) of NaOH was dissolved in 500 mL of methanol. To this solution was added 18.2 g (80 mmol) of myristic acid. The solution became clearer, but white aggregates remained. The mixture was stirred for 15−20 min at room temperature. Meanwhile, 8.2 g (26 mmol) of cadmium nitrate tetrahydrate was dissolved in 50 mL of methanol. This solution was added to the sodium myristate solution. A white precipitate was formed very rapidly. After 15 min of stirring at

room temperature, the white solid was isolated by filtration, washed three times with methanol ,and dried overnight under vacuum.

Preparation of Cadmium Oleate ($Cd(OA)_2$) 0.5 M. A solution of cadmium oleate 0.5 M in oleic acid was synthesized by heating 1.28 g of CdO in 20 mL of oleic acid at 160 °C under argon for 1 h until the mixture turned colorless. The solution was then degassed under vacuum at 70 °C for 30 min.

Preparation of SODE 0.1 M. Sulfur stock solution in ODE (SODE 0.1 M) was prepared by heating 320 mg of sulfur in 100 mL of degassed ODE at 120 °C until complete dissolution.

CdSe/CdS Quantum Dots. In a three neck flask, 170 mg of $Cd(Myr)_2$ and 7.5 mL of ODE were degassed under vacuum for 30 min at room temperature. Then the atmosphere was switched to Ar and the temperature raised to 240 °C. While the temperature rose, 3 mL of ODE and 36 mg of Se powder were mixed together. After brief sonication, 1 mL of the Se solution was injected into the flask. After 5 min, a mixture of 3 mL of ODE and 100 μL of oleic acid was injected dropwise over 3 min. The temperature was then set to 260 °C to grow the CdS shell. Ten milliliters of oleylamine and 10 mL ODE were injected in the flask. Meanwhile, a mixture of 36.6 mL of SODE at 0.1 M and 7.3 mL of $Cd(OA)_2$ 0.5 M in ODE was prepared. Thirteen milliliters of the previous solution was injected dropwise at 9 mL/h. Then 18 mL of the same solution was injected at 18 mL/h. The flask was then brought back to room temperature. The content of the flask was split into two Falcon tubes with 0.5 mL of oleic acid in each. Ethanol was added to precipitate the particles. After centrifugation, the particles were redispersed in fresh hexane. The cleaning procedure was repeated two further times.

The obtained particles had a first excitonic feature just below 600 nm and a final size of (11 $\pm$ 1) nm, with a typical core diameter of 3 nm; absorption and luminescence spectra, as well as TEM images of the synthesized QDs are available in Figure S1 of the Supporting Information.

Sample Preparation. BK7 microscopy cover slides were placed in a 2% aqueous solution of Hellmanex and cleaned in a heated (50 °C) ultrasonic bath for 30 min. The substrates were then rinsed with pure water and dried in the spin coater for 120 s at v = 8000 rpm. A 50 μL drop of the diluted QD stock solution (90/10 hexane/octane) was deposited on the dry samples while they were spinning at a constant v = 6000 rpm.

Experimental Setup. All experiments were carried out with a home-built wide-field microscope, a sketch of which is presented in Figure 1a and, with more detail, in Figure S2 of the Supporting Information. The excitation laser was a 561 nm continuous-wave solid state laser (Spectra-Physics Excelsior), coupled into a single-mode fiber to ensure a zero-order Gaussian excitation beam. The laser was collimated by a 15.4 mm aspheric lens and focused by a 250 mm achromatic doublet onto the back focal plane of an oil-immersion microscope objective (Olympus, NA = 1.35, f = 3 mm) after passing through a polarizing beam splitter (PBS). This geometry resulted in a Gaussian excitation spot on the sample surface with a full width at half-maximum (fwhm) of around 33 μm. The sample of CdSe/CdS quantum dots spin-coated onto a microscopy coverslip could be positioned with a precision of a few tens of nanometers by means of an XYZ piezo stage (PI NanoCube). The photoluminescence (PL) of the excited QDs was collected by the same objective and passed through the PBS, which acted as a first-stage (OD 3) laser suppression. A 90:10 (reflection/transmission) beam splitter transmitted 10% of the collected light to a CCD camera through an f = 100 mm achromat, allowing observation of the laser spot on the sample surface with 33$\times$ magnification. An optional bandpass filter at (593 $\pm$ 20) nm could be inserted in front of the CCD camera to select the QD emission, which is centered at 597 nm. The remaining 90% of QD photoluminescence passed through the same type of bandpass filter and were focused onto the cathode of an electron-bombarded CMOS (ebCMOS) camera[43−45] by a f = 1 m plano-convex lens, resulting in 333$\times$ magnification. Taking into account the collection efficiency of the objective of about 60%, half of the PL being rejected by the PBS and the 10% quantum efficiency (QE) of the ebCMOS sensor at 600 nm, the overall collection efficiency was estimated as $\beta \approx 3\%$.

Simulation of Power-Law Blinking. The details of our numerical simulations of power-law blinking, which took into account all experimental conditions and constraints, are given in the Supporting Information.

Conflict of Interest: The authors declare no competing financial interest.

Acknowledgment. We acknowledge technical support by J. Margueritat, J.-F. Sivignon, Y. Guillin, and the Lyon center for nano-opto technologies (NanOpTec). This research was supported by the Programme Avenir Lyon Saint-Étienne (ANR-11-IDEX-0007) of Université de Lyon, within the program "Investissements d'Avenir" operated by the French National Research Agency (ANR). J. Houel thanks the Fédération de Recherche André Marie Ampère (FRAMA) for financial support. This work was performed in the context of the European COST Action MP1302 NanoSpectroscopy.

Supporting Information Available: Experimental techniques, numerical simulations, and further capability benchmarks of our approach. This material is available free of charge *via* the Internet at http://pubs.acs.org.

REFERENCES AND NOTES

1. Nirmal, M.; Dabbousi, B. O.; Bawendi, M. G.; Macklin, J. J.; Trautman, J. K.; Harris, T. D.; Brus, L. E. Fluorescence Intermittency in Single Cadmium Selenide Nanocrystals. *Nature* **1996**, *383*, 802–804.
2. Banin, U.; Bruchez, M.; Alivisatos, A. P.; Ha, T.; Weiss, S.; Chemla, D. S. Evidence for a Thermal Contribution to Emission Intermittency in Single CdSe/CdS Core/Shell Nanocrystals. *J. Chem. Phys.* **1999**, *110*, 1195–1201.
3. Kuno, M.; Fromm, D. P.; Hamann, H. F.; Gallagher, A.; Nesbitt, D. J. Nonexponential "Blinking" Kinetics of Single CdSe Quantum Dots: A Universal Power Law Behavior. *J. Chem. Phys.* **2000**, *112*, 3117–3120.
4. Shimizu, K. T.; Neuhauser, R. G.; Leatherdale, C. A.; Empedocles, S. A.; Woo, W. K.; Bawendi, M. G. Blinking Statistics in Single Semiconductor Nanocrystal Quantum Dots. *Phys. Rev. B* **2001**, *63*, 205316.
5. Frantsuzov, P.; Kuno, M.; Janko, B.; Marcus, R. A. Universal Emission Intermittency in Quantum Dots, Nanorods and Nanowires. *Nat. Phys.* **2008**, *4*, 519–522.
6. Klimov, V. I.; Mikhailovsky, A. A.; Xu, S.; Malko, A.; Hollingsworth, J. A.; Leatherdale, C. A.; Eisler, H. J.; Bawendi, M. G. Optical Gain and Stimulated Emission in Nanocrystal Quantum Dots. *Science* **2000**, *290*, 314–317.
7. Anikeeva, P. O.; Halpert, J. E.; Bawendi, M. G.; Bulovic, V. Electroluminescence from a Mixed Red-Green-Blue Colloidal Quantum Dot Monolayer. *Nano Lett.* **2007**, *7*, 2196–2200.
8. Lounis, B.; Bechtel, H. A.; Gerion, D.; Alivisatos, P.; Moerner, W. E.Photon Antibunching in Single CdSe/ZnS Quantum Dot Fluorescence. *Chem. Phys. Lett.* **2000**, *329*, 399–404.
9. Michler, P.; Imamoglu, A.; Mason, M. D.; Carson, P. J.; Strouse, G. F.; Buratto, S. K. Quantum Correlation among Photons from a Single Quantum Dot at Room Temperature. *Nature* **2000**, *406*, 968–970.
10. Brokmann, X.; Hermier, J. P.; Messin, G.; Desbiolles, P.; Bouchaud, J. P.; Dahan, M. Statistical Aging and Nonergodicity in the Fluorescence of Single Nanocrystals. *Phys. Rev. Lett.* **2003**, *90*, 120601.
11. Lutz, E. Power-Law Tail Distributions and Nonergodicity. *Phys. Rev. Lett.* **2004**, *93*, 190602.
12. Randall, J. T.; Wilkins, M. H. F. Phosphorescence and Electron Traps. 2.The Interpretation of Long-Period Phosphorescence. *Proc. R. Soc. A* **1945**, *184*, 390–407.
13. Tang, J.; Marcus, R. A. Diffusion-Controlled Electron Transfer Processesand Power-Law Statistics of Fluorescence Intermittency of Nanoparticles. *Phys. Rev. Lett.* **2005**, *95*, 107401.
14. Kuno, M.; Fromm, D. P.; Hamann, H. F.; Gallagher, A.; Nesbitt, D. J. "On"/"Off" Fluorescence Intermittency of Single Semiconductor Quantum Dots. *J. Chem. Phys.* **2001**, *115*, 1028–1040.

15. Kuno, M.; Fromm, D. P.; Johnson, S. T.; Gallagher, A.; Nesbitt, D. J. Modeling Distributed Kinetics in Isolated Semiconductor Quantum Dots. *Phys. Rev. B* **2003**, *67*, 125304.
16. Verberk, R.; van Oijen, A. M.; Orrit, M. Simple Model for the Power-Law Blinking of Single Semiconductor Nanocrystals. *Phys. Rev. B* **2002**, *66*, 233202.
17. Margolin, G.; Protasenko, V.; Kuno, M.; Barkai, E. Power-Law Blinking Quantum Dots: Stochastic and Physical Models. *Adv. Chem. Phys.* **2006**, *133*, 327–356.
18. Frantsuzov, P. A.; Marcus, R. A. Explanation of Quantum Dot Blinking without the Long-Lived Trap Hypothesis. *Phys. Rev. B* **2005**, *72*, 155321.
19. Lippitz, M.; Kulzer, F.; Orrit, M. Statistical Evaluation of SingleNano-Object Fluorescence. *ChemPhysChem* **2005**, *6*, 770–789.
20. Sher, P. H.; Smith, J. M.; Dalgarno, P. A.; Warburton, R. J.; Chen, X.; Dobson, P. J.; Daniels, S. M.; Pickett, N. L.; O'Brien, P. Power Law Carrier Dynamics in Semiconductor Nanocrystals at Nanosecond Timescales. *Appl. Phys. Lett.* **2008**, *92*, 101111.
21. Goldstein, M. L.; Morris, S. A.; Yen, G. G. Problems with Fitting to the Power-Law Distribution. *Eur. Phys. J. B* **2004**, *41*, 255–258.
22. Hoogenboom, J. P.; den Otter, W. K.; Offerhaus, H. L. Accurate and Unbiased Estimation of Power-Law Exponents from Single-Emitter Blinking Data. *J. Chem. Phys.* **2006**, *125*, 204713.
23. Clauset, A.; Shalizi, C. R.; Newman, M. E. J. Power-Law Distributions in Empirical Data. *SIAM Rev.* **2009**, *51*, 661–703.
24. Riley, E. A.; Hess, C. M.; Whitham, P. J.; Reid, P. J. Beyond PowerLaws: A New Approach for Analyzing Single Molecule Photoluminescence Intermittency. *J. Chem. Phys.* **2012**, *136*, 184508.
25. Crouch, C. H.; Sauter, O.; Wu, X. H.; Purcell, R.; Querner, C.; Drndic, M.; Pelton, M. Facts and Artifacts in the Blinking Statistics of Semiconductor Nanocrystals. *Nano Lett.* **2010**, *10*, 1692–1698.
26. Watkins, L. P.; Yang, H. Detection of Intensity Change Points inTime-Resolved Single-Molecule Measurements. *J. Phys. Chem. B* **2005**, *109*, 617–628.
27. Pelton, M.; Grier, D. G.; Guyot-Sionnest, P. Characterizing Quantum-Dot Blinking Using Noise Power Spectra. *Appl. Phys. Lett.* **2004**, *85*, 819–821.
28. Pelton, M.; Smith, G.; Scherer, N. F.; Marcus, R. A. Evidence for a Diffusion-Controlled Mechanism for Fluorescence Blinking of Colloidal Quantum Dots. *Proc. Natl. Acad. Sci. U.S.A.* **2007**, *104*, 14249–14254.
29. Messin, G.; Hermier, J. P.; Giacobino, E.; Desbiolles, P.; Dahan, M. Bunching and Antibunching in the Fluorescence of Semiconductor Nanocrystals. *Opt. Lett.* **2001**, *26*, 1891–1893.
30. Verberk, R.; Orrit, M. Photon Statistics in the Fluorescence of Single Molecules and Nanocrystals: Correlation Functions *versus* Distributions of On- and Off-Times. *J. Chem. Phys.* **2003**, *119*, 2214–2222.
31. Bardou, F.; Bouchaud, J.-P.; Aspect, A.; Cohen-Tannoudji, C. *Lévy Statistics and Laser Cooling: How Rare Events Bring Atoms to Rest*;Cambridge University Press: Cambridge, 2002.
32. Peacock, J. A. Two-Dimensional Goodness-of-Fit Testing in Astronomy. *Mon. Not. R. Astron. Soc.* **1983**, *202*, 615–627.
33. Fasano, G.; Franceschini, A. A Multidimensional Version of the Kolmogorov-Smirnov Test. *Mon. Not. R. Astron. Soc.* **1987**, *225*, 155–170.
34. Knappenberger, K. L.; Wong, D. B.; Romanyuk, Y. E.; Leone, S. R. Excitation Wavelength Dependence of Fluorescence Intermittency in CdSe/ZnS Core/Shell Quantum Dots. *Nano Lett.* **2007**, *7*, 3869–3874.
35. Mahler, B.; Spinicelli, P.; Buil, S.; Quélin, X.; Hermier, J. P.; Dubertret, B. Towards Non-Blinking Colloidal Quantum Dots. *Nat. Mater.* **2008**, *7*, 659–664.
36. Orrit, M. Chemical and Physical Aspects of Charge Transfer in the Fluorescence Intermittency of Single Molecules and Quantum Dots. *Photochem. Photobiol. Sci.* **2010**, *9*, 637–642.
37. Canneson, D.; Biadala, L.; Buil, S.; Quélin, X.; Javaux, C.; Dubertret, B.; Hermier, J. P. Blinking Suppression and Biexcitonic Emission in Thick-Shell CdSe/CdS Nanocrystals at Cryogenic Temperature. *Phys. Rev.B* **2014**, *89*, 035303.
38. Galland, C.; Brovelli, S.; Bae, W. K.; Padilha, L. A.; Meinardi, F.; Klimov, V. I. Dynamic Hole Blockade Yields Two-Color Quantum and Classical Light from Dot-in-Bulk Nanocrystals. *Nano Lett.* **2013**, *13*, 321–328.
39. Javaux, C.; Mahler, B.; Dubertret, B.; Shabaev, A.; Rodina, A. V.; Efros, A. L.; Yakovlev, D. R.; Liu, F.; Bayer, M.; Camps, G.; *et al.* Thermal Activation of Non-Radiative Auger Recombination in Charged Colloidal Nanocrystals. *Nat. Nanotechnol.* **2013**, *8*, 206–212.
40. Wang, X. Y.; Ren, X. F.; Kahen, K.; Hahn, M. A.; Rajeswaran, M.; Maccagnano-Zacher, S.; Silcox, J.; Cragg, G. E.; Efros, A. L.; Krauss, T. D. Non-Blinking Semiconductor Nanocrystals. *Nature* **2009**, *459*, 686–689.
41. Malko, A. V.; Park, Y. S.; Sampat, S.; Galland, C.; Vela, J.; Chen, Y. F.; Hollingsworth, J. A.; Klimov, V. I.; Htoon, H. Pump-Intensity- and Shell-Thickness-Dependent Evolution of Photoluminescence Blinking in Individual Core/Shell CdSe/CdS Nanocrystals. *Nano Lett.* **2011**, *11*, 5213–5218.
42. Goushi, K.; Yamada, T.; Otomo, A. Excitation Intensity Dependence of Power-Law Blinking Statistics in Nanocrystal Quantum Dots. *J. Phys. Chem.C* **2009**, *113*, 20161–20168.
43. Barbier, R.; Cajgfinger, T.; Calabria, P.; Chabanat, E.; Chaize, D.; Depasse, P.; Doan, Q. T.; Dominjon, A.; Guérin, C.; Houles, J.; *et al.* A Single-Photon Sensitive ebCMOS Camera: The LUSIPHER Prototype. *Nucl. Instrum. Methods Phys. Res., Sect. A* **2011**, *648*, 266–274.
44. Doan, Q.; Barbier, R.; Dominjon, A.; Cajgfinger, T.; Guérin, C. Multiple-Target Tracking Implementation in the ebCMOS Camera System:The LUSIPHER Prototype. *Proc. SPIE* **2012**, *8436*, 84360J.
45. Guérin, C.; Mahroug, J.; Tromeur, W.; Houles, J.; Calabria, P.; Barbier, R. An Acquisition System for CMOS Imagers with a Genuine 10 Gbit/s Bandwidth. *Nucl. Instrum. Methods Phys. Res., Sect. A* **2012**, *695*, 420–424.